Northwest Atlantic Fisheries Organization

Serial No. N7549 **NAFO SCR Doc. 24/042**

SCIENTIFIC COUNCIL MEETING – JUNE 2024

Optical, Chemical, and Biological Oceanographic Conditions in the Labrador Sea from summer 2019 and 2023

M. Ringuette, E. Devred, K. Azetsu-Scott, E. Head, C.-E. Gabriel, and S. Clay

Ocean and Ecosystem Sciences Division, Science Branch
Department of Fisheries and Oceans
Bedford Institute of Oceanography
P.O. Box 1006, 1 Challenger drive
Dartmouth, Nova Scotia B2Y 4A2

ABSTRACT

The chemistry and biology of the Labrador Sea and adjacent shelves have undergone significant changes over the 2019–2023 period compared to previous years. The Atlantic Zonal Off-shelf Monitoring Program (AZOMP) revealed an increase in dissolved inorganic carbon and a decrease in pH, a trend that extends back to the beginning of the monitoring program in the mid-1990's. While the mean concentration of chlorofluorocarbon (CFC-12) over the water column has remained stable, the concentration of sulfur hexafluoride (SF_6) has been increasing steadily since we began to measure it in 2011, reflecting the atmospheric history of these gases. The mean temperature of the top layer (0–100 m) has been mainly below normal since 2011, except for the Hamilton Bank where two warmer-than-normal years were observed in 2015 and 2018, and in the Central Labrador Sea when mean temperature was above normal in 2012. In 2019, the entire Labrador Sea temperature was above normal with a record-high mean temperature in the Central Labrador Sea, while mean temperature was below normal in 2022. The shelves mean temperature were close to normal in 2023 and the Central Labrador Sea temperature was above-normal. In the 2019-2023 period, both surface and deep nutrients levels were below normal except for the Greenland Shelf in 2022 and surface silicate in 2023, however, the timing of the mission with respect to the spring phytoplankton bloom development may impacts the nutrient budget. In fact, the timing of the mission before 2019 occurred earlier each year compared to the previous year due to the constraints of crew change, and consistent dates in sea-going expeditions are needed to remove uncertainties related to sampling time. Deep nutrients exhibited inter-annual and regional variations until 2018. In recent years (2019-2023), deep-nutrients have remained below average in all three regions of interest, suggesting a profound change in the biogeochemistry of the Labrador Sea.

While integrated chlorophyll-a levels were below normal in 2019, continuing a trend that started in 2014, except in 2015 in the Central Labrador Sea, values in 2022 and 2023 were above average, with a record-high integrated chlorophyll-a value in 2022 on the Hamilton Bank. An unusually large bloom of *Phaeocystis* sp., that covered a large extent of the Labrador Sea, occurred in 2022 and explains the high values. This is the second largest *Phaeocystis* sp. bloom event in the Labrador Sea after 2015. Satellite-derived chlorophyll-a

concentration reveals the large variability in the peak timing of the spring bloom and in the fall bloom initiation. While the mean annual satellite-derived chlorophyll-a on Hamilton Bank was mainly above-normal, values were below-normal between 2019-2021 on the Greenland Shelf and Central Labrador Sea, and above normal in 2022-2023.

Unfortunately, the late (2020) or lack of (2021) in situ data collection due to the COVID pandemic and the lack of ship availability, respectively, did not allow inclusion of these two years in the current report with the exception of satellite ocean color metrics, such that recent in situ trends need to be interpreted with caution.

INTRODUCTION

The Labrador Sea is a deep basin nested between Labrador and Greenland with a cyclonic circulation pattern that leads to the mixing of Arctic and North Atlantic waters. The Baffin Island and Labrador currents transport cold and less-saline Arctic water southward along the Canadian coast (Wang et al. 2016). On the eastern side, the West Greenland Current brings warmer, more-saline waters northward, along the Greenland coast into the Baffin Bay, where it meets the Labrador Current. (See Lozier et al. 2019 and Yashayaev et al. 2017 for a detailed description of the Labrador Sea circulation.) By the end of winter, the cooling of the upper layer results in an increase of surface density, enabling wind-driven mixing to reach great depths (1500 to 2000 m), thus ventilating the deeper ocean with atmospheric gases while pumping nutrients from the deep waters to the surface. The intensity of this phenomenon varies with environmental factors, including atmospheric forcing, freshwater runoff from adjacent glaciers, precipitation, intrusion of warm and saline inflow from the adjacent North Atlantic, and intrusion of cold and fresh water from the Arctic Ocean. In turn, this deep mixing strongly impacts heat flux, stratification, and by extension, the chemical balance and biological productivity of the Labrador Sea. Consequently, changes in the physical and chemical environment of the aphotic zone influence both plankton community composition and annual biological production cycles, including fish and higher trophic levels.

About one quarter of carbon dioxide (CO_2) released by human activities is taken up by the oceans (Sabine et al. 2004), altering ocean chemistry, and correspondingly, the marine carbonate system. The Labrador Sea hosts a strong "solubility pump", whereby anthropogenic CO_2 sequestrated from the atmosphere is transported to the deep ocean through chemical and physical processes. The dissolution of anthropogenic CO_2 has decreased ocean pH by 0.1 units over the past 200 years, resulting in a 30% increase in acidity (Caldeira and Wickett 2003). If global emissions of CO_2 remain at their present rate, ocean pH is predicted to drop by an additional 0.3 units by 2100. The oceans have not experienced such a rapid pH decrease (ocean acidification), or one of such a high magnitude, for at least 20 million years (Feely et al. 2004), raising serious concerns about the ability of marine ecosystems to adapt. The major impact of decreasing pH will be felt by organisms that form calcium carbonate ($CaCO_3$) shells and skeletons, because rising acidity increases the solubility of $CaCO_3$. Since $CaCO_3$ shells and skeletons are naturally more soluble at lower temperatures and higher pressures, high latitudes and deep water ecosystems, such as the one encountered in the Labrador Sea, are more vulnerable to the added stress of ocean acidification than those at intermediate latitudes. Furthermore, rapid environmental changes, such as receding sea-ice extent and enhanced hydrological cycles, may amplify these problems. Inert halogenated trace gases of anthropogenic origin that have accumulated in the atmosphere, such as the chlorofluorocarbons (CFCs) and sulfur hexafluoride (SF_6), are used to study ventilation and transport processes in the ocean. In recent decades, they have been used to calculate Transient Tracer Distribution (TTD) to estimate the transit time of water masses and anthropogenic CO_2 in the water (Haine and Hall 2002; Hall et al. 2002).

Since 1990, as part of the World Ocean Circulation Experiment (WOCE), the Ocean and Ecosystem Sciences Division (OESD) at the Bedford Institute of Oceanography (BIO) has carried out an annual occupation, usually in the spring, of the AR7W (Atlantic Repeat Hydrography Line 7 West) oceanographic section across the Labrador Sea (Figure 1). Soon after its inception, the program morphed into Fisheries and Oceans Canada (DFO) Atlantic Zone Off-shelf Monitoring Program (AZOMP), following the OESD's overarching objectives to: 1) characterize and understand the causes of ocean variability at seasonal, inter-annual, and inter-decadal scales; 2) provide adequate data to monitor the health of the marine ecosystem and support decision-making based on scientific evidence; and 3) to build historical databases to address future issues. The program also contributes to the international Global Climate Observing System (GCOS) and the Climate Variability (CLIVAR) component of the World Climate Research Program (WCRP) and it reports annually with an environmental synopsis to the Northwest Atlantic Fisheries Organization (NAFO).

The AR7W section spans approximately 900 km across the southern edge of the Labrador Sea, from the Labrador Shelf (near 53°N) to the Greenland Shelf (near 61°N) (Figure 1). The annual AZOMP multidisciplinary survey of the Labrador Sea primarily consists of AR7W occupations and deployments/recoveries of moorings and Argo floats. The ideal timing of the mission in May aims to capture the fading winter-deep-convection signal and the beginning of the phytoplankton bloom and productivity season, while avoiding possible sea-ice on the Labrador Shelf early in the spring. Sampling the peak of the spring bloom is uncertain given its large inter-annual variability in timing, duration and spatial extent,

however, early cruise dates in recent decades have captured its initiation with the exception of the 2021 mission, which occurred in July-August under nutrient-limited conditions (Table 1, Figure 2). With nearly three decades of measurements, the time series allows examination of decadal trends in all key ecosystem variables (i.e, temperature, nutrients, plankton biomass and abundance).

The AR7W transect crosses two productive shelves (Labrador and Greenland Shelves) and the Central Labrador Sea, where phytoplankton production is subject to local forcing (eddies, mixing-stratification) that drive phytoplankton biomass and community structure. In the Central Labrador Sea, light limits primary production for most of the year (Harrison and Li 2008; Fragoso et al. 2016), while a shallow mixed layer and relatively low nitrate concentration limit phytoplankton growth on the Labrador Shelf following the spring bloom. Phytoplankton growth, in particular diatoms, also seemed to be limited by availability of silicate in the Central Labrador Sea (Harrison and Li 2008). These conditions support the emergence of small flagellates such as *Phaeocystis pouchetii* in the northern and eastern region of the Labrador Sea, which can form large blooms under favorable conditions (Fragoso et al. 2016). In recent years, large blooms of *Phaeocystis* sp. have also been observed in the western part of the Central Labrador Sea (Devred et al. 2024). The Labrador Shelf, influenced by Arctic waters, is dominated by polar diatom species (*Thalassiosira* spp., *Chaetoceros* spp., and *Bacteriosira bathyomphala*) and species associated with sea-ice (*Porosira glacialis* and *Fossula arctica*). Primary production patterns and mesoscale features leave their imprint on the mesozooplankton distribution and abundance (Yebra et al. 2009). One species of copepod, *Calanus finmarchicus*, dominates the mesozooplankton biomass throughout the central region of the Labrador Sea, while on the shelves, two Arctic *Calanus* species, *C. glacialis* and *C. hyperboreus*, are equally important (Head et al. 2003). *C. finmarchicus* abundance shows regional variations that are generally consistent from year-to-year and are related to differences in the timing of life-cycle events, which are influenced by environmental conditions, including spring bloom dynamics.

This report describes the biogeochemical state of the Labrador Sea between spring 2019 and spring 2023. Data presented in this report come from: 1) annual surveys carried out over 2-week periods, typically between early May and early June, however, due to the unavailability and subsequent decommissioning of CCGS Hudson, the timing of the surveys in 2020 occurred in summer between late July and early August and there was no mission in 2021 (Table 1) ; and 2) satellite remote-sensing of daily observations of ocean colour converted into chlorophyll-a (chl-a) concentration.

DATA SOURCES AND METHODS OF ANALYSIS

The following section describes the data sources and sampling methods used for the estimation of the biogeochemical variables and indices depicted in the present report.

In situ Samples collection

Core stations

The core stations (Figure 1) remain the priority of the monitoring program to ensure geographical consistency over time when reporting on the data. The main goal of the sampling is to obtain a complete suite of measurements at selected locations from surface to bottom to characterize the physical and chemical properties of the entire water column and the biological properties in the upper layers (0 to 100m). The CTD (Conductivity, Temperature, Depth)-rosette system used to carry out measurements and water collection includes twelve 24 L Niskin bottles and a core of twinned sensors to measure temperature, salinity and oxygen, as well as additional sensors to measure fluorescence (both chl-a and Colored Dissolved Organic Matter (CDOM)), pH, light attenuation, Photosynthetically Active Radiation (PAR) and current velocity (LADCP). Water samples are collected at 24 depths distributed over the entire water column to measure transient gasses (CFC and SF_6), oxygen, partial pressure of carbon dioxide (pCO2), Total Inorganic Carbon (TIC), alkalinity, pH, nutrients, and salinity. In addition to the previous measurements, four surface-layer depths (2, 25, 50 and 100 m) are sampled for chl-a and cell abundance (Flow Cytometry). The 2-m depth is sampled for phytoplankton absorption and pigment composition, particulate carbon, and CDOM absorption. Once the CTD-Rosette is onboard, the collection of water from the Niskin bottles is carried out as listed

previously (i.e., gases first and phytoplankton last) from bottom to surface waters to minimize the loss of transient tracers and other gases during sampling. All variables were sampled and analyzed following GO-SHIP protocols (Hood et al. 2010; Mitchell et al. 2002). In addition to water sampling from the Niskin bottles, mesozooplankton are collected in vertical net hauls in the upper 100 m using a 0.75 m diameter ring net fitted with a 200 µm mesh, and 0.5 m diameter ring net with a 76 µm mesh size. A detailed description of the processing of the physical oceanographic data is presented in Yashayaev et al. 2020.

When time allows, extra stations are added between core stations in order to increase the spatial resolution of the sampling. However, on these stations only measurements from the sensors located on the CTD-Rosette are recorded and water is not collected unless requested by programs outside the core program. At these stations, the CTD-Rosette system is lowered to the ocean bottom to profile the entire water column. Note that in the current report, only data collected on the core and biological stations are included.

Biological stations

The purpose of these stations is to increase the vertical resolution compared to core stations and to carry out Photosynthesis-Irradiance (P-I) 14C-uptake experiments with phytoplankton (water) samples. In these experiments, 33 aliquots of phytoplankton from two depths (surface and close to the deep chl-a maximum) are incubated with 14C-bicarbonate at in situ temperatures and 30 light levels (+ 3 dark bottles) for approximately 3 hours. The P-I measurements are used to estimate primary production according to Platt and Jassby (1976). The actual location of the biological stations is not critical, so the vessel is stopped mid-morning during transit between stations, in order to start the incubations around noon, local time, to ensure consistency of the method. Because the biological stations focus on the upper layers of the water column, the CTD sensor is only lowered to 200 m, allowing for a greater vertical resolution of all the biogeochemical parameters. Bottles are closed at 2, 10, 20, 30, 40, 50, 60, 80, 100, and 150 m, with an extra bottle at the depth of the deep chl-a maximum, as revealed by the in situ fluorescence sensor. In general, a total of seven biological stations are sampled, which are spread along the AR7W transect: two on the Labrador Shelf, three in the Central Labrador Sea, and two on the Greenland Shelf.

Discrete variable measurements and Data collection

Transient Tracers SF_6 and CFC-12

Prior to analysis, seawater samples from the rosette were drawn directly into 250 mL glass syringes and were stored at approximately 4 °C in a low-temperature incubator for up to 12 hours. Immediately before analysis, the samples were warmed to approximately 20 °C in a water bath then injected into the purge vessel of a custom-made purge-and-trap system, where dissolved gases were stripped from the sample in a stream of ultra-high-purity nitrogen with a flow rate of 140 mL per minute. The SF_6 and CFC-12 gases were quantitatively retained in a trap comprised of 30 cm of 1/16" stainless steel tubing packed with 100–120 mesh Carboxen 1000, held at -70 °C over liquid nitrogen. After each 7 minute purge cycle, the trap was heated to 180 °C with a low-voltage electric current and the desorbed gases directed to a Varian gas chromatograph equipped with an electron-capture detector. SF_6 and CFC-12 were separated on a one-meter pre-column packed with Porasil B and a three-meter main column packed with Molecular Sieve 5A held isothermally at 100 °C. Total run-time was 11.5 minutes. The chromatographic sample peaks were quantified with Varian Galaxie software and the analytical system calibrated at least once each day using an air standard supplied by the Climate Monitoring and Diagnostics Laboratory of the National Oceanic and Atmospheric Administration (CMDL/NOAA), Boulder, Colorado. Analytical precision, as determined by repeated standard injections, was around ± 2% for SF_6 and ± 0.7% for CFC-12.

pH Measurements

Seawater was analyzed for pH according to spectrophotometric Standard Operating Procedure 6b (SOP 6b) described in *Guide to best practices for ocean CO_2 measurements* (Dickson et al. 2007). Water was collected from the rosette in 60 mL borosilicate glass tubes, allowing each sample to overflow by at least one volume.

Samples were stored in a low-temperature incubator at 4 °C prior to analysis. The maximum time between sampling and analysis was about 4 hours. Racks of tubes were then placed in a water bath held at 25 °C and allowed to thermally equilibrate for 30 minutes. Each sample was then introduced into a water-jacketed 10 cm quartz cell and 30 µL of the purified indicator dye m-cresol purple added before mixing well. The absorbance of light at the wavelengths 434 and 578 nm was measured with an Agilent photodiode array spectrophotometer and the resulting extinction coefficients at these wavelengths were used to determine the pH of the sample. The performance of the spectrophotometer was monitored by daily measurements of a trisaminomethane (Tris) buffer solution of known pH.

Total Inorganic Carbon (TIC) and Total Alkalinity (TA)

Seawater samples were collected in 500 mL borosilicate glass bottles and preserved with mercuric chloride following the method described in *Guide to best practices for ocean CO_2 measurements* (Dickson et al. 2007). Total Inorganic Carbon (TIC) was determined after return to BIO's chemical laboratory using gas extraction and coulometric titration with photometric endpoint detection (Johnson, et al. 1985). Total alkalinity (TA) was measured by open-cell potentiometric titration with full curve Gran Point determination using a Titrando dosimat with Tiamo software, in conjunction with a sample-delivery system built in-house. Certified Reference Material (CRM) (supplied by Professor Andrew Dickson, Scripps Institution of Oceanography, San Diego, USA) was analyzed in duplicate at intervals to calibrate for accuracy.

Discrete pCO2

Water samples for pCO_2 measurements were drawn from the rosette (following dissolved oxygen) into 160 mL volume crimp seal vials, allowing each sample vial to overflow by about 3 volumes before immediately preserving with 50 µL of saturated mercuric chloride solution and crimp sealing with butyl rubber septa. The samples were stored at 4 ºC and analyzed at BIO's chemical laboratory upon return. Surface samples were collected at every station throughout the cruise and two full-depth profiles were collected from Stations 17 and 18 on the AR7W line. pCO2 was later determined by headspace equilibrium gas chromatography with flame ionization detection, using the method of Neill et al. (1997).

Surface temperature (Surface to 100 m)

CTD profiles were collected between the surface and near bottom (often several thousand meters deep), however, in this report only temperature collected from the 0–100 m range is used, which is the most relevant to interpret the biological sampling. CTD profiles are binned at 1 m resolution and the arithmetic average is computed to provide a single temperature value per profile for the 0–100 m layer. The first few meters from the downward cast are generally not recorded, due to the requirement for sensors to acclimate underwater (3 min at 10m deep). Following the acclimation period, the instrument is brought as close as possible to the surface but, partly because of the ship's movements, the sensors do not reach the theoretical 0 m depth. Surface values are obtained by linear extrapolation of the temperatures at the two depths closest to the surface (e.g., 2 and 3 m) and this value is included in the mean temperature. Following the surface measurement, the CTD is lowered to the bottom at a speed of 30 m/min for the first hundred meters and at a speed of 60m/min for the rest of the cast. An altimeter is used to reach about a 5 m elevation over the seafloor, at which the first bottle is closed and the CTD starts its ascent.

Nutrients

Nutrient measurements were made using a SEAL Analytical continuous-flow AutoAnalyzer 3 (AA3) and concentrations are expressed in micromoles per liter. The analytical methods have been modified from the historically used Technicon II: Technicon for Seawater Analysis (Silicate 186 72W, Phosphate 155 71W, Nitrate/Nitrite 158 71W) (Kérouel and Aminot 1997) so as to remain compatible with methods described in the nutrient section of *The GO-SHIP Repeat Hydrography Manual* (Becker et al. 2019). Duplicate nutrient samples were drawn into 10 ml collection vials directly from the rosette without using tubing, with

technicians wearing vinyl gloves to avoid contamination. Samples were stored at 4 ˚C and analyzed within 12 hours. Five dissolved inorganic nutrients were analyzed, namely, nitrate plus nitrite (NO_3 + NO_2), nitrite (NO_2), phosphate (PO_4), silicate (SiO_4), and ammonium (NH_4). Note that in 2023, nutrients were frozen and analyzed upon return to BIO due to a lack of laboratory space in the CCS Jacques Cartier preventing the installation of the auto-analyser.

The instrument was calibrated for every analytical run, using a six-point calibration curve from pre-made solutions diluted using artificial seawater of same salinity as the samples, distributed over the concentration range for each nutrient. The analysis was followed by a drift standards analysis and blank samples to determine the method's detection limits. The baseline was re-assessed every 12 sample duplicates (i.e., every 6 samples). The pH of the imidazole buffer was monitored to ensure optimal pH levels for the nitrate plus nitrite analyses, and adjusted as needed using hydrochloric acid, thus improving the lifespan and stability of the cadmium reduction column. Ultimately, this method diminished drift issues observed in the past between analytical runs.

The quality of these analyses was validated by analyzing a CRM for nutrients produced by KANSO Co., Ltd, Japan. There is no existing reference material for ammonium in seawater, although CRM values were tracked for consistency.

In situ Chlorophyll-a concentration

Phytoplankton biomass is represented by the concentration of its main pigment, chl-a, which was measured using Turner fluorometry (Yentsch and Menzel 1963). Details of the protocol and method can be found in Mitchell et al. (2002). In brief, two replicates of 100 ml aliquots of seawater were drawn from each sampling depth and filtered via vacuum filtration (PSI < 10) onto 25 mm glass fiber filters (GF/F). The GF/Fs were immediately deposited into separate scintillation vials containing 10 ml of 90% acetone, which were kept at -20 °C for at least 24 hours to ensure extraction of all the chl-a pigments. Following the extraction period, the aliquots were warmed to room temperature and transferred into fluorometer cuvettes (glass test tubes). The extracts were exposed to blue light (excitation wavelengths) in the fluorometer, which leads them to emit red light. This red light is detected and quantified by a photomultiplier (Holm-Hansen et al. 1965). Chloropigments other than chl-a (e.g., chlorophyll-b, chlorophyll-c1, -c2, and -c3) can contribute to the overall fluorescence signal, but their contribution is generally minor. Chl-a degradation products (a-type phaeopigments associated with senescent phytoplankton or zooplankton fecal pellets) may sometimes be present in a sample and contribute to the fluorescent signal. To account for their contribution, after taking the first fluorescence measurement, samples were acidified, which converts chl-a into phaeophytin-*a*. A conversion factor was then applied to retrieve the concentrations of both the chl-a and a-type phaeopigments (Welschmeyer 1994).

Satellite-derived Chlorophyll-a concentration

In addition to in situ measurements, chl-a concentrations were derived using satellite ocean colour. This mode of observation provides information on phytoplankton biomass at synoptic scales and daily frequency (assuming clear skies). These satellite-derived data are used to complement the in-situ observations by providing context to the seagoing missions, including a suite of metrics to characterize the phytoplankton spring bloom (see section 4.12). Satellite data presented in this document are retrieved using the MODerate Resolution Imaging Spectroradiometer (MODIS) on the Aqua platform launched by the National Aeronautic Space Administration (NASA) in 2002. While NASA has launched several satellites since 1998, in this report only data from the MODIS sensor are presented in order to have a consistent and climate-compatible time series of chl-a concentrations that is free of satellite inter-calibration issues. MODIS is the satellite with the longest continuous time series—the first full year of data was 2003 and it is still operating.

For this report, global daily level-3 binned data at 4 km resolution were downloaded from NASA Ocean Biology Processing Group and data were extracted for the three regions of interest, namely, Hamilton Bank (HB, -55.7°E to -53.7°E and 53.6°N to 55.5°N), the Central Labrador Sea (CLS, -53.7°E to -48.8°E and 55.5°N to 60.1°N), and the Greenland Shelf (GS, -48.8°E to -48.1°E and 60.1°N to 60.7°N) (Figure 1). Remote sensing

reflectances were used to generate POLY4 chl-a (Clay et al, 2019), a modified version of the band ratio model OCx (O'Reilly et al, 1998) with regionally-tuned coefficients to correct a bias observed in the Northwest Atlantic. Mapped POLY4 data for the Northwest Atlantic are available online, hosted by CIOOS Atlantic (https://cioosatlantic.ca/erddap/info/bio_remote_sensing_modis_aqua_chl_poly4/index.html).

Mesozooplankton

Mesozooplankton were collected using vertical net hauls in the upper 100 m, where 95% of the biomass in spring-summer occurs (Astthorsson and Gislason 2003), using a 0.75 m diameter ring net fitted with a 200 µm mesh size and 0.5 m diameter ring net with a 76 µm mesh size. The cod-end was attached via a clamp to a weighted hydro-wire and the towing bridle was attached to a crossbow mounted on the wire, at a height above the cod-end such that the net was held vertically. In this configuration, zooplankton were only collected as the net was towed upwards. The towing speed was about 0.5 m s^{-1} and the volume of water sampled was assumed to be the volume of the cylinder sampled by the net, until 2010, when the filtered volumes started to be measured using a Danemark K/C flowmeter. The flowmeter was equipped with a back-spin pin, to prevent the impeller from spinning during the descent of the net, so that it only measured flow during the ascent. Samples were preserved in 2% formalin. For *C. finmarchicus*, *C. hyperboreus*, and *C. glacialis*, specimens were identified and enumerated to the level of species and stage, and size-frequency distributions of sizes-at-stage were constructed for all stages at each station. Other taxa were identified to the level of species (sometimes to stage), genus, or group, depending on their abundance in the samples. Meaningful abundances were obtained when a minimum of 300 organisms, and a minimum of 200 *Calanus* spp., were counted to allow assessment of community structure and *Calanus* population growth/development, respectively.

Computational methods

Spatio-temporal binning

All data are aggregated following a spatio-temporal scheme to summarise the information in simple metrics. For the biogeochemical data, three main regions are considered (Figure 1), the 1) Hamilton Bank (HB), located on the Labrador Shelf, 2) the Central Labrador Sea and 3) the Greenland Shelf.

All nutrients and chl-a concentrations were integrated over selected depth ranges, namely, chl-*a* from 0 to 100 m, surface nutrients from 0 to 100 m and deep nutrients from the first depth below 100 m to bottom. Temperatures were averaged from 0 to 100 m. Zooplankton values correspond to the integrated abundances in the water column (0–100 m) since collection was carried out using vertical net tows. (See Section 4.9.). Following the vertical binning, the data were averaged by region and year.

Time series

AZOMP sampling period is dictated by the Canadian Coast Guard operational needs and ship availability, which has been challenging since the late 2010's due to mechanical issues with the research vessel CCGS Hudson. From 2008 to 2018 (except 2013), AZOMP missions have started slightly early each year, with about 25 days difference over the entire period (Figure 2). The timing of the mission has been very variable since 2019 with the chartering of oceanographic vessels to conduct the mission. In addition, the COVID pandemic in 2020 prevented the chartering of foreign vessels and the mission was only possible on the CCGS Amundsen at a later date in July – August (Table 1). As a result, measurements collected during that mission were not included in the analysis to avoid possible bias.

Scorecards

Annual anomalies for temperature, surface and deep nutrients, chl-a concentration, mesozooplankton abundance, and satellite ocean colour metrics were calculated as the deviation of an individual year from the mean of the annual estimates over a reference period (1999-2010 for mesozooplankton and 1999–2020 for

the remaining in situ data, and 2003-2020 for satellite data), and expressed as normalized quantities (i.e., by dividing by the standard deviation of the annual estimates over the same period):

$$A_y = (M_y - M_r) / (\sigma_r)$$

where A_y is the anomaly for a given property in a given year (y) and region, M_y is the annual mean, M_r is the reference period mean and σ_r is the standard deviation for the reference period. This method was selected because it provides good estimates of anomalies and trends for data with large gradients and gaps (Jones and Hulme 1995).

Spring bloom metrics

Metrics were derived from satellite chl-a using the PhytoFit R shiny app (https://cioosatlantic.ca/phytofit). Data were $\log_{10}$-transformed to allow better modelling of the exponential increase in chl-a at the initiation of the bloom. Daily averages and standard deviations were calculated within each Labrador Sea polygon, filtering pixels outside ±3standard deviations from the mean. Days with less than 20% coverage were excluded from the time series, and the remaining points were smoothed using the LOESS method (locally-estimated scatterplot smoothing) as implemented in R (l*oess()* function) with a span window of 0.2 (a parameter that controls the degree of smoothing) and weighted by percent coverage. A symmetric shifted Gaussian was fitted to the smoothed points with nonlinear least squares regression using the *nlsLM()* function of the *minpack.lm* package in R, and the chl-a baseline was allowed to vary linearly as a function of time. The Gaussian fits were restricted to days 85 to 299, and the day of initiation and day of maximum concentration were restricted to day ranges 85-226 and 108-247, respectively to avoid classification of small early peaks of the spring bloom.

In previous reports, the spring bloom metrics relied mainly on the Gaussian fit (the timing of the start of the bloom, the duration, peak concentration during the bloom period, and "magnitude" or total chl-a produced during the bloom period), which were subject to high variability in chl-a concentration and low data coverage, particularly in the north early in the year. This resulted in an absence of model fits, or problematic fits that may not have accurately captured the interannual anomalies in each region. To reduce the impact of these bad fits on the scorecards, and retrieve information about bloom timing and intensity, a new set of a metrics were recently proposed: spring bloom peak timing and fall bloom initiation, and "seasonal" averages, where the season boundaries are region-specific and based on the climatology of the spring and fall bloom periods observed over the time series (Blais et al., in prep). While the spring metrics are still derived from a Gaussian fit, we now report on the peak of the curve instead of its initiation, as it does not require a subjective threshold (i.e., percentage of maximum chl-a) and it remains robust to small variation in chl-a early in spring. All fits were visually inspected to ensure that the bloom peak timing was accurately captured by the model, and the input parameters were adjusted if necessary.

The fall bloom period is less predictable than the spring bloom as it signal is not as large as in the spring and satellite data are more sparse due to cloud cover. Rather than a Gaussian model, a threshold method was used to determine the start of the bloom as the day of year when chl-a concentration surpasses 105% of the annual median and remains above this threshold for 14 consecutive days (Layton et al, 2021). In this case we used the LOESS-smoothed data spanning between day of year 151 and 365 with the initiation occurring between day of year 151 to 270. The timing of the fall bloom initiation was reported rather than the peak, as the peak may occur late in the year when data coverage is poor. Annual times series at daily resolution and the corresponding spring Gaussian and fall threshold fits are available at github.com/BIO-RSG/PhytoFit/blob/master/verified_fits.

The mean chl-a for the spring and fall was calculated as an average of the daily chl-a concentrations during the two periods mentioned above, weighted by percent coverage. Note that in this calculation, daily chl-a concentrations correspond to the averages calculated using absolute (i.e. not log-transformed) values within the polygons, after filtering outlying pixels. Data coverage is very sparse or non-existent in the Labrador Sea from November to January (see Figure 13). Days with valid data that have low coverage (<20%), a common

occurrence early or late in the year, might not be representative of the overall conditions. Sea ice also impacts the quality of the data and may introduce artifacts close to the ice edge (Bélanger et al., 2007). Although weighting points by percent coverage lessens the impact of low data coverage, extra caution must be used when interpreting results in late fall or winter due to these issues.

Access to Data Products

Data products presented in the figures of this document are published on the Government of Canada's Open website; a link to the data is available on request to the corresponding author. The bloom metrics estimated from satellite ocean colour data in each of the three regions presented in Figure 9 are available in the github repository for the PhytoFit app (https://github.com/BIO-RSG/PhytoFit/tree/master/verified_fits). All the chemical data are available at Ocean Carbon Data System (OCADS).

RESULTS AND DISCUSSION

Total Inorganic Carbon and pH

The Labrador Sea hosts a strong "solubility pump"—atmospheric anthropogenic CO_2 is sequestrated to the deep ocean by chemical and physical processes. The depth of the Newly Ventilated Labrador Sea Water (NV-LSW) trapped by winter convection varies from year to year, ranging from 500 m to over 2000 m. The average concentrations of TIC and pH, between 150 and 500 m for stations from 56°N to 59.1°N (within the Central Labrador Sea), were used as representative concentrations for NV-LSW and suffered relatively less from seasonal variability. TIC concentration increased by 0.78 μmol kg^{-1} y^{-1} from 1996 to 2023, reaching a maximum of 2167.92 μmol kg^{-1} in 2022 in response to the local uptake of anthropogenic CO_2 (Figure 3). As a result, the pH decreased by 0.09 units during the same period (Figure 3) representing a decline rate of 0.003 y^{-1}. Trends between 1996 and 2023 were highly significant with a correlation coefficient, r^2, explaining respectively 97% and 84% of the variance in TIC and pH. Arctic outflow and the local uptake of anthropogenic CO_2 in the deep-convection region of the Labrador Sea are major controlling mechanisms for the state of ocean acidification in the northwest Atlantic, and the continuous trend observed in our dataset could impact this entire region. The Arctic water inflows to the highly productive regions in the northwest Atlantic, which have important commercial fisheries and make these regions more susceptible to future ocean acidification than other regions (Azetsu-Scott et al. 2010). Ocean acidification also influences the capacity of the ocean to take up CO_2 from the atmosphere.

Transient tracers CFC-12 and SF_6

During the second half of the twentieth century, the atmospheric burden of CFCs increased steadily, due mainly to their widespread use as refrigerants and aerosol propellants. The invasive atmospheric flux of these mostly inert gases provided an excellent record of ocean circulation, and profiles of dissolved CFC-12 concentration have been measured annually along the AR7W line since 1991 (Figure 4). As a consequence of restrictions on the manufacturing and use of ozone-depleting substances introduced in 1989, the atmospheric mixing ratio of CFC-12 has been in decline since 2003 and its capacity at tracking recent ventilation episodes has become limited (Figure 4). Measurements of an alternative transient tracer, SF_6, were introduced in 2011. There has been a rapid, near-linear increase in atmospheric SF_6 since 2011 and it is reflected in the dissolved concentration profiles of the recently ventilated water, represented by the layer of the Central Labrador Sea between 150 and 500m (Figure 4), compared with CFC-12.

Temperature in the top 100 m

Temperatures recorded by the CTD during the occupation were averaged between 0 and 100 m, which corresponds roughly to the temperature regime of the phyto- and mesozoo- plankton sample layer. Because the timing of the cruise affects the average temperature for a given region and year, removal of the 2003 and 2004 (due to later-than-usual sampling dates, Figure 2) from the reference period lowered it by about 0.2 °C

with little effect on the anomaly patterns (not shown here). HB exhibited a lower temperature (mean of 0.8 °C) than the CLS (mean of 3.8 °C) and the GS (mean of 2.3 °C) due to the inflow of Arctic water (Figure 5).

The CLS warmest year occurred in 2000 (+1.67 standard deviations from the mean, unitless), while the warmest anomaly for the GS happened in 2008 (+1.92) (Figure 5). The coolest year on the HB occurred in 1996 (-2.12) and in 2018 on the CLS (-1.51). The HB and CLS show year-to-year variability between 2019 and 2023 with 2019 being the warmest recorded anomaly in the CLS (+1.47). The GS showed negative anomalies in 2022 and 2023, a trend that started in 2011 (except 2019), perhaps with less intensity in recent years. In 2023, both shelves exhibited temperature slightly lower than normal, while the CLS showed temperature higher than normal. Unfortunately, the lack of data in 2020, and a late mission in 2021, did not allow confirmation of these trends.

Nutrients

All near-surface nutrient concentrations (i.e., 0–100 m, nitrate, phosphate, and silicate) exhibited inter-annual variations between 1997 and 2010, followed by three years (2011 to 2013) of below average nutrient levels for all regions except the silicate concentration in 2011 on HB (Figure 6). From 2014 to 2018, all nutrients levels were above normal except for nitrate and phosphate in 2015 in CLS. While no patterns are observed between nutrients and regions before 2011, all regions and nutrients anomalies were correlated between 2011 and 2019.

Since 2019, surface nitrates show negative trends in all three regions, except on the Greenland Shelf in 2022 (Figure 6). The same year, a record-low in nitrate was measured in the CLS. The same trends were observed in phosphate anomalies between 2019 and 2023 with lower than usual concentrations in both the HB and CLS, and a record low phosphate in the CLS in 2023. Silicate levels show a different pattern with more variability than nitrate and phosphate levels. HB showed lower than normal silicate levels since 2019 with a record low in 2022. Silicate levels were close to normal in the CLS. In 2019, silicate were lower than normal on the GS and higher than normal in 2022 and 2023.

Deep nutrients (100+ m to bottom) showed a different pattern than the surface nutrients in agreement with the hydrodynamics of the Labrador Sea and the surface-layer biological activity (Figure 7). Deep nutrients levels are less impacted by the timing of the mission as they are not consumed by phytoplankton and microbial remineralization at depth replenishes the nutrient pool. Deep nutrients anomalies showed large interannual variability between 1999 and 2018 (Figure 7), interestingly most of the record-high levels occurred in the first half of the time series, except for nitrate and silicate on HB, which occurred in 2015, a notable year given an unusual large bloom of *Phaeocystis* sp. (Devred et al., 2024). On the other hand, record-low levels of nutrients occurred after 2009. While no clear trend has emerged for the scorecards, since 2019 all deep nutrients have showed below-average levels. However, this trend should be interpreted with caution given that no data from 2020 and 2021 are included. It is noteworthy that these below-average levels of nutrients that started in 2019 coincided with the trend for surface nutrients (Figures 6 and 7).

***In situ* Chlorophyll-a concentration**

In general, the GS region has high levels of integrated chl-a with a mean of 380 mg m^{-2} (Figure 8), and is dominated by nanophytoplankton with low concentrations of picophytoplankton. Conversely, the CLS is a region with low integrated chl-a (165 mg m^{-2}) and a low proportion of nanophytoplankton, with high concentrations of picophytoplankton. The HB region exhibits the lowest concentrations of integrated chl-a (122 mg m^{-2}) and micro- and nano-phytoplankton dominates the phytoplankton assemblage, with low biomass of picophytoplankton. Upper ocean (<100 m depth) phytoplankton sampled on the AR7W section in spring and early summer between 1999 and 2022 showed region-specific characteristics (Li and Harrison 2014, Fragoso et al. 2016 Devred et al., 2024).

Integrated chl-a shows a low frequency variability with a given trend (above or below average) that remains for several years at a time. In that respect, the time series for the HB and CLS show two periods of lower-than-normal levels, from about 2001 to 2005 and from 2014 to 2019, while the remaining periods show above-normal values. Record-high level of integrated chl-a occurred in 2022 (+3.48) on the HB and in 2015 in the

CLS. Note that both years corresponds to very large blooms of *Phaeocystis* sp. The GS showed a different pattern than the two other regions, with lower than normal values between 2001 and 2008, followed by a period of large interannual variability (2009 to 2013, 2009 being the record high). Since 2014, integrated chl-a has been lower than average.

Regarding the period of interest in the current report, 2019 to 2023, integrated chl-a showed lower than normal levels in 2019 in all three regions, continuing a trend that started in 2014 (except in Central Labrador Sea in 2015, Figure 8). This trend was also observed in 2022 and 2023 on the Greenland Shelf, although the integrated chl-a was close to normal in 2023. The HB and CLS showed higher than normal levels in 2022 and 2023, with a record high value in 2022 on the CLS.

Integrated chl-a levels do not necessarily agree with nutrients concentrations, which can be somewhat explained by the timing of the missions (Figure 2). For instance, in 2013, the mission sampled the transect at the peak of the bloom (as indicated by satellite ocean colour), resulting in high integrated chl-a and low nutrients, likely depleted by phytoplankton consumption. Conversely, in 2014, the mission sampled the AR7W before or at the start of the spring bloom, when chl-a concentration was low and nutrients levels high. Similarly, both 2021 and 2022 missions on HB and in the CLS occurred at the peak of the spring bloom (Figure 2), corresponding to high integrated chl-a values and low nutrients values.

Satellite-derived Chl-a and bloom indices

Satellite-derived chl-a allows observation of the Labrador Sea all year long, but is limited by sea-ice and cloud cover. The main advantage of the satellite is that information on phytoplankton biomass can be reported when sea-going missions have been cancelled. Here we report on the timing of the spring and fall blooms, and annual and seasonal mean chl-a in the three regions of interest.

The timing of the spring bloom is highly variable and depends on several factors, including the thermal stratification, the amount of nutrients, the light available for photosynthesis and the grazing pressure. The spring bloom generally occurs first on the GS (day of year (doy) 135 on average), then on the HB (doy 153 on average) and shortly after in the CLS (doy 160 on average). There are no long term trends observed in the timing of the spring bloom but rather a strong interannual variability. Following the record-late spring initiation in 2018 on HB, both 2019 and 2020 also showed a late bloom, while 2021, 2022 and 2023 showed an earlier than normal bloom initiation. In the CLS, the bloom initiation was late from 2019 to 2021, the later year exhibiting the record-late bloom, which was followed by a record-early bloom in 2022. Note that in 2022, a very large and unusual bloom of *Phaeocystis* sp. was observed (Devred et al., 2024). In 2023, the spring bloom initiation occurred later than normal. In fact, the 2022 bloom was the only one observed to occur earlier than normal since 2016. On the GS, both 2019 and 2021 showed earlier than normal bloom initiation, while it was later than normal for the other years. The spring bloom in 2023 was the record-late timing on the GS. A secondary bloom occurs in the Fall, less intense than the spring one, triggered by the replenishment in nutrients of the surface-lit layer by storm-induced vertical mixing when light is still sufficient to stimulate phytoplankton productivity. Similar to the spring bloom peak timing, the fall bloom initiation is very variable over the time series and for each region. Overall, the fall bloom timing has been earlier than normal since 2012, except for a few late years in each regions. On HB, the bloom was earlier than normal in 2019, 2020 and 2021, while it was later than normal in 2022, but exhibiting a record early timing in 2023. In the CLS, the fall bloom occurred earlier than usual in all years, however no fall bloom was observed in 2021. On the GS, the fall bloom timing showed a similar pattern to HB, with an extremely late fall bloom (anomaly of 1.42).

Annual and spring anomalies show correlation in all three regions, suggesting that the spring bloom drives the annual production. The mean annual and seasonal chl-a shows a high interannual variability. Examining the anomalies in recent years (2019 to 2023), HB exhibited a record high annual chl-a average (+2.03) despite lower than average levels of nitrate and silicate, suggesting that the ecosystem is not nutrient-limited. The mean annual chl-a was above average in all three regions in 2023 in spring. CLS showed above normal chl-a in 2022, in particular in spring, due to an anomalously large bloom of *Phaeocystis* sp. The GS showed the lowest production of the 2019-2023 period in 2020 when mean chl-a was below normal in all seasons except in summer with a relatively high anomaly. In winter, 2022 showed a record-high mean chl-a in the GS. An

exceptionally large bloom occurred in 2018 on the HB and CLS (3.92 and 3.97, respectively) impacting the entire reference period and reducing the anomalies for all the other years.

Mesozooplankton

Updates from the period currently reported are not yet available, but we have decided to leave the historical sections up to 2019. *Calanus finmarchicus* copepods dominate the mesozooplankton biomass in the Central Labrador Sea, while it and its congeners *C. glacialis* and *C. hyperboreus* contribute about one third each on the shelves (Head et al. 2003). *C. finmarchicus* total abundances are greatly influenced by the abundance of young stage copepodites. These develop from eggs laid by females that have overwintered as pre-adults in the deep central basin and re-ascended in spring. The spring bloom provides the food to fuel egg-laying and subsequent population development, so that regional differences in spring bloom dynamics also lead to differences in the timing of the development of *C. finmarchicus* populations. Since spring blooms are generally earlier and more intense on the GS than elsewhere, *C. finmarchicus* populations are generally more abundant there than elsewhere at the time of in situ sampling (Figure 10).

On the Labrador Shelf, during the 1995 to 2018 period, there were two years with exceptionally high abundances for *C. finmarchicus*–1999 (June) and 2011 (May)—the reasons for which are unknown (Figure 10). Otherwise, abundances have been variable, with two higher-than-average values (June 2001 and July 2002) and a sustained period of relatively-low abundance between 2004 and 2008. Since 2013, abundances have been slightly below average.

In the Central Labrador Sea, because the spring bloom and the relatively late development of *C. finmarchicus*, *in situ* sampling in summer generally gave higher abundances than in spring, as indicated by the positive anomalies in 1995, 1999, 2002, and 2003 (Figure 10). Young stages were seldom very abundant, perhaps due to high mortality (Head et al. 2015), except for the summer of 1995, with an exceptionally higher total abundance year. There was no trend in spring time total abundance for *C. finmarchicus* between 1996 and 2014. Since 2015, however, abundances have been unusually low, perhaps owing to earlier sampling than in previous years (Figures 2 and 10).

On the Greenland Shelf, there was one exceptionally high *C. finmarchicus* abundance value in May 2006, the cause of which is unclear. Otherwise, higher-than-average values tended to be associated with later sampling dates (e.g., 1995, 1999, 2001–2003, and 2012), while relatively low abundances were associated with early sampling dates since 2012.

High abundance of *C. glacialis* and *C. hyperboreus* on the shelves may result from the transport of individuals in the inflows, since neither species have a local overwintering source population. The abundances of both species have generally shown considerable year-to-year variability, but with sustained periods of low abundance for *C. glacialis* on both shelves since 2014, and sustained periods of high abundance for *C. hyperboreus* on the GS between 2009 and 2012 and of low abundance on the LS since 2014. *C. hyperboreus* abundance on the GS was also low in 2018 (Figure 10).

Clausocalanidae, mainly represented here by the genius *Pseudocalanidae* spp., were persistently more abundant than the average in the CLS over the last 10 years, whereas a general decreasing trend was observed on LS and GS since 2014 (Figure 11). Unlike *Pseudocalanidae*, *Oithonidae* were persistently less abundant in the Central Labrador Sea for more than 10 years, while the decrease in abundance on both shelves became more prevalent around 2014 (Figure 11). Since 2014, *Euphausiid* abundances have been consistently lower than average in all regions (Figure 12). Amphipods, mostly represented here by *Parathemisto libellula*, showed higher-than-average abundances in the Central Labrador Sea in 2018. Being a species associated with Arctic water masses, this phenomenon is consistent with the cooler-than-average temperatures in the Central Labrador Sea during that year (Figure 12).

SUMMARY

The Atlantic Zone Off-Shelf Monitoring Program (AZOMP) provides observations on ocean climate and plankton variability within the Labrador Sea and adjacent shelves affecting ecosystems of Atlantic Canada and

climate from a regional to global scale. In the Labrador Sea, surface heat losses in winter result in the formation of dense waters, which spread across the ocean, ventilating the deep layers, thus contributing to the global ocean-overturning circulation. Since 2014, the mid-high latitude North Atlantic experienced moderate to high surface heat loss leading to elevated convective mixing during the winter period, and significant formation of Labrador Sea Water (LSW), among the highest in terms of volume and depth.

Strong inter-annual variability was observed in surface nutrient concentrations, which are consistent among regions. Since 2014, there have been positive anomalies in all regions, with a trend that started in 2013 in the CLS for nitrate, phosphate, and silicate. The CLS showed a below-average nitrate concentration in 2015, however, likely as a result of the nutrient draw down caused by the abnormally large bloom observed in that year. Negative anomalies have been observed on HB and CLS in 2022 and 2023, breaking the trend of high anomalies. Chl-a concentrations have followed an inverse pattern, with lower than normal concentrations for all three regions since 2014, except for the anomalously high concentration in 2015, and high concentrations on HB and CLS in 2022-2023. The high anomalies in 2015 and 2022 were associated with an intense phytoplankton bloom consisting mainly of *Phaeocystis* sp. which was identified from shipboard observations. Ocean color metrics (spring peak timing, fall bloom initiation, and annual and seasonal averages) showed no obvious trends over time and each region revealed its own pattern. Satellite observations are impacted by cloud cover, resulting in data gaps which might miss the peak of the bloom in a given year and region. Recurrent earlier sampling dates from year to year may partly explain the observed negative anomalies in in-situ chl-a concentrations, since sampling may have occurred before the start of the seasonal spring bloom.

The 0–100 m abundances of several mesozooplankton taxa followed a pattern similar to that shown by phytoplankton (chl-a) concentration, with lower-than-average abundances since 2014. For some taxa this may be linked in part to their seasonal life-cycles, since earlier sampling in recent years means that the populations were less developed (i.e., include fewer members of the new year's generation). Interestingly, the unusually intense bloom of 2015 did not appear to have any effect on the abundances of any of the mesozooplankton taxa.

ACKNOWLEDGEMENTS

The authors thank the sea-going staff of the Bedford Institute of Oceanography and the officers and crew of the Canadian Coast Guard ships Amundsen and Captain Jacques Cartier as well as the UNOLS research vessel Atlantis. Jay Barthelotte, Robert Benjamin, Jay Bugden, Diana Cardoso, Carla Caverhill, Darlene Childs Terry Cormier, Melissa Falkner, Jennifer Field, Pascal Guillot, Adam Hartling, Dave Hebert, Flo Hum, Jeff Jackson, Matt Lawson, Chantelle Layton, Dave Levy, Richard Nelson, Kevin MacIsaac, Kevin Pauley, Tim Perry, Cathy Porter, Steve Punshon, Maddison Proudfoot, Peter Thamer Christiane Theriault, Mike Vining and Kristen Wilson contributed to sample collection, sample analysis, data analysis, data management, and data sharing.

REFERENCES CITED

Astthorsson, O.S., and Gislason, A. 2003. Seasonal variations in abundance, development and vertical distribution of Calanus finmarchicus, C. hyperboreus and C. glacialis in the East Icelandic Current. Journal of Plankton Research 25(7): 843–854.

Azetsu-Scott, K., Clarke, A., Falkner, K., Hamilton, J., Jones, E.P., Lee, C., Petrie, B., Prinsenberg, S., Starr, M. and Yeats, P. 2010. Calcium Carbonate Saturation States in the waters of the Canadian Arctic Archipelago and the Labrador Sea. Journal of Geophysical Research 115: C11021.

Becker, S., Aoyama, M., Woodward, E.M.S., Bakker, K., Coverly. S., Mahaffey, C. and Tanhua, T. 2019. GO-SHIP Repeat Hydrography Nutrient Manual: The precise and accurate determination of dissolved inorganic nutrients in seawater, using Continuous Flow Analysis methods. In: The GO-SHIP Repeat Hydrography Manual: A Collection of Expert Reports and Guidelines.

Bélanger S., Ehn J.K., Babin M., Impact of sea ice on the retrieval of water-leaving reflectance, chlorophyll a concentration and inherent optical properties from satellite ocean color data, Remote Sensing of Environment, Volume 111, Issue 1, 2007, p. 51-68, https://doi.org/10.1016/j.rse.2007.03.013

Caldeira, K., and Wickett, M.E. 2003. Anthropogenic carbon and ocean pH. Nature.425: 365

Clay, S.; Peña, A.; DeTracey, B.; Devred, E. Evaluation of Satellite-Based Algorithms to Retrieve Chlorophyll-a Concentration in the Canadian Atlantic and Pacific Oceans. Remote Sens. 2019, 11, 2609. https://doi.org/10.3390/rs11222609

Denman, K. L. and Platt, T. 1975. Coherences in the horizontal distributions of phytoplankton and temperature in the upper ocean. Mem. Soc. r. Sci. Liège 6e série 7: 19–30.

Devred E., Wilson K. L., Perry T., Hardy M., Brosnahan M., and Ringuette M. 2024. Identification and validation of phytoplankton taxonomic assemblages derived from pigment signatures using samples collected in the Labrador Sea from 2014 to 2022. Can. Tech. Rep. Fish. Aquat. Sci. 3596: viii + 55 p.

Dickson, A.G., Sabine, C.L. and Christian, J.R. (Eds.) 2007. Guide to Best Practices for Ocean CO2 Measurements. PICES Special Publication 3. 191 pp.

Feely, R.A., Sabine, C.L., Lee, K., Berelson, W., Kleypas, J., Fabry, V.J., and Millero, F.J. 2004. Impact of Anthropogenic CO2 on the CaCO3 System in the Oceans. Science. 305(5682): 362–366.

Fragoso, G.M., Poulton, A.J., Yashayaev, I.M., Head, E.J.H., Stinchcombe, M.C., and Purdie, D.A. 2016. Biogeographical patterns and environmental controls of phytoplankton communities from contrasting hydrographical zones of the Labrador Sea. Progress in Oceanography 141: 212–226.

Gillard, L. C., Hu, X., Myers, P. G. and Bamber, J. L. 2016. Meltwater pathways from marine terminating glaciers of the Greenland ice sheet. Geophysical Research Letters. 43:10,873-10,882.

Haine, T. W. N., and Hall, T.M. 2002. A generalized transport theory: Water mass composition and age. Journal Physical Oceanography. 32:1932–1946.

Hall, T. M., Haine, T. W. N. and Waugh, D. W. 2002. Inferring the concentration of anthropogenic carbon in the ocean from tracers. Global Biogeochemical Cycles. 16(4):1131. https://doi.org/10.1029/2001GB001835

Harrison, W.G. and Li, W.K.W. 2008. Phytoplankton growth and regulation in the Labrador Sea: light and nutrient limitation. J. Northwest. Atl. Fish. 39:71–82.

Hátún, H., Azetsu-Scott, K., Somavilla, R., Rey, F., Johnson, C., Mathis, M., Mikolajewicz, U., Coupel, P., Tremblay, J.-É., Hartman, S., Pacariz, S.V., Salter, I., and Ólafsson, J. 2017. The subpolar gyre regulates silicate concentrations in the North Atlantic. Scientific Reports 7(1): 14576.

Head, E.J.H., Gentleman, W.C., and Ringuette, M. 2015. Variability of mortality rates for Calanus finmarchicus early life stages in the Labrador Sea and the significance of egg viability. Journal of Plankton Research 37(6): 1149–1165.

Head, E.J.H., Harris, L.R., and Yashayaev, I. 2003. Distributions of Calanus spp. and other mesozooplankton in the Labrador Sea in relation to hydrography in spring and summer (1995–2000). Progress in Oceanography 59(1): 1–30.

Holm-Hansen, O., Lorenzen, C.J., Holmes, R.W., and Strickland, J.D.H. 1965. Fluorometric Determination of Chlorophyll. ICES Journal of Marine Science 30(1): 3–15.

Hood, E.M., Sabine, C.L. and Sloyan, B.M. (eds) 2010. The GO-SHIP Repeat Hydrography Manual: a collection of expert reports and guidelines, Version 1. (IOCCP Report 14), (ICPO Publication Series 134).

Johnson, K.M., Sieburth, J.M., Williams, P.J. leB, and Brändström, L. 1987. Coulometric total carbon dioxide analysis for marine studies: Automation and calibration. Marine Chemistry 21(2): 117–133.

Jones, P.D., and Hulme, M. 1996. Calculating regional climatic time series for temperature and precipitation: methods and illustrations. International Journal of Climatology 16(4): 361–377. John Wiley & Sons, Ltd.

Kérouel, R., and Aminot, A. 1997. Fluorometric determination of ammonia in sea and estuarine waters by direct segmented flow analysis. Marine Chemistry 57(3): 265–275.

Layton, C, Devred, E and B DeTracey. 2021. A comparison of phytoplankton spring bloom fitting methods using MODIS satellite-derived chlorophyll-a concentration for the Maritimes region, Can. Tech. Rep. Hydrogr. Ocean Sci. ###: vii + 22 p

Li, W.K.W. and Harisson, W.G. 2014. The state of phytoplankton and bacterioplankton in the Labrador Sea: Atlantic Zone Off-Shelf Monitoring Program 1994–2013. Can. Tech. Rep. Hydrogr. Ocean. Sci. 302:xviii+181p.

Lozier, M.S., et al. 2019. A sea change in our view of overturning in the subpolar North Atlantic. Science 363(6426): 516.

Luo, H., Castelao, R.M., Rennermalm, A.K., Tedesco, M., Bracco, A., Yager, P.L., and Mote, T.L. 2016. Oceanic transport of surface meltwater from the southern Greenland ice sheet. Nature Geoscience 9(7): 528–532.

Mitchell, M.R., Harrison, G., Pauley, K., Gagné, A., Maillet, G., and Stain, P. 2002. Atlantic zonal monitoring program sampling protocol. Can. Tech. Rep. Hydrogr. Ocean Sci. 223: iv + 23p.

Neill, C., Johnson, K.M., Lewis, E., and Wallace, D.W.R. 1997. Accurate headspace analysis of fCO2 in discrete water samples using batch equilibration. Limnology and Oceanography 42(8): 1774–1783.

O'Reilly, John & Maritorena, S. & Mitchell, B.G. & Siegel, David & Carder, Kendall & Garver, S.A. & Kahru, Mati & Mcclain, Charles. (1998). Ocean color chlorophyll algorithms for SeaWiFS. Journal of Geophysical Research. 103. 937-953.

Platt, T. and Jassby, A.D. (1976), The relationship between photosynthesis and light for natural assemblages of coastal marine phytoplankton. Journal of Phycology 2: 421–430.

Richardson, A.J., Walne, A.W., John, A.W.G., Jonas, T.D., Lindley, J.A., Sims, D.W., Stevens, D., and Witt, M. 2006. Using continuous plankton recorder data. Progress in Oceanography 68(1): 27–74.

Sabine, C.L., Feely, R.A., Gruber, N., Key, R.M., Lee, K., Bullister, J.L., Wanninkhof, R., Wong, C.S., Wallace, D.W.R., Tilbrook, B., Millero, F.J., Peng, T.-H., Kozyr, A., Ono, T., and Rios, A.F. 2004. The Oceanic Sink for Anthropogenic CO2. Science 305(5682): 367.

Stephanie Clay, Chantelle Layton, & Emmanuel Devred. (2021). BIO-RSG/PhytoFit: First release (v1.0.0). Zenodo. https://doi.org/10.5281/zenodo.4770754

Wang, Z., Brickman, D., Greenan, B.J.W., and Yashayaev, I. 2016. An abrupt shift in the Labrador Current System in relation to winter NAO events. Journal of Geophysical Research: Oceans 121(7): 5338–5349.

Welschmeyer, N.A. 1994. Fluorometric analysis of chlorophyll a in the presence of chlorophyll b and pheopigments. Limnology and Oceanography 39(8): 1985–1992.

Yashayaev, I., and Loder, J.W. 2017. Further intensification of deep convection in the Labrador Sea in 2016. Geophysical Research Letters 44(3): 1429–1438.

Yashayaev, I., Peterson I., and Wang Z. 2020. Meteorological, Sea Ice and Physical Oceanographic Conditions in the Labrador Sea during 2018. DFO Can. Sci. Advis. Sec. Res. Doc. 2020/nnn. v + 36 p.

Yebra, L., Harris, R.P., Head, E.J.H., Yashayaev, I., Harris, L.R., and Hirst, A.G. 2009. Mesoscale physical variability affects zooplankton production in the Labrador Sea. Deep Sea Research Part I: Oceanographic Research Papers 56(5): 703–715.

Yentsch, C., and Menzel, D. 1963. A Method for the Determination of Phytoplankton Chlorophyll and Phaeophytin by Fluorescence. Deep-Sea Research 10(3): 221–231.

Zhai, L., Platt, T., Tang, C., Sathyendranath, S., and Walls, R.H. 2011. Phytoplankton phenology on the Scotian Shelf. ICES J. Mar. Sci. 68(4): 781–791.

TABLES

Table 1. Atlantic Zone Off-Shelf Monitoring Program sampling missions between 2014 and 2018.

Year	Mission ID	Dates	# Hydro Stations	# BIO Stations	# Net Stations
2019	AMU2019-001	9 – 21 June	55	7	40
2020	AMU2020-001	28 July – 7 August	62	7	36
2021	Mission cancelled	5 – 15 May	0	0	0
2022	AT4805	10-20 May	62	7	28
2023	CAR2023-573	26 May – 6 June	35	0	35

FIGURES

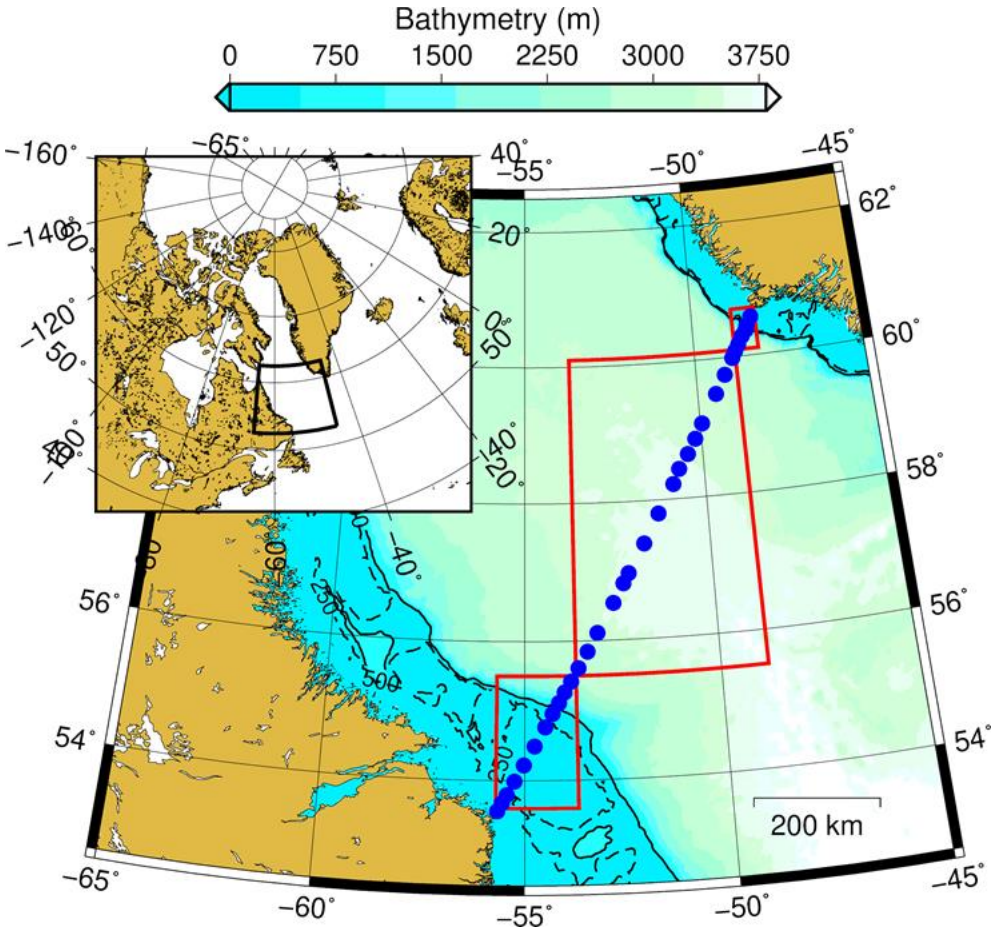

Figure 1. AR7W transect within the Labrador Sea. Blue dots represent the location of the core stations. Red boxes correspond to the regions where satellite chl-a concentration is extracted (i.e., Hamilton Bank, Central Labrador Sea, and Greenland Shelf). Solid and dashed black lines correspond to the 500 and 250 m isobaths, respectively.

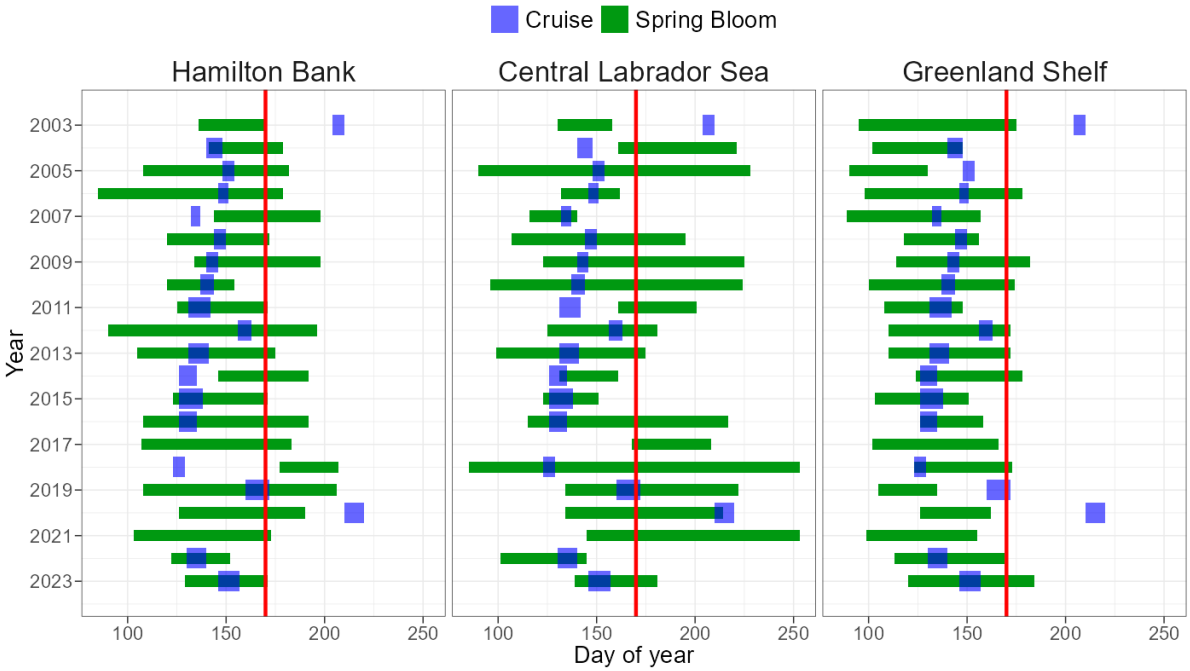

Figure 2. Blue rectangles represent the sampling period (actual occupation of AR7W line) and green rectangles correspond to the duration of the spring bloom within each region as derived from satellite ocean colour. Dates are reported in day of year. The COVID pandemic prevented the execution of the mission in 2020. Vessel availability lead to the absence of a mission in 2017. Mission in 2019 and 2020 onboard CCGS Amundsen respectively in late June and August. Vertical red line represents our cutoff date separating spring and summer (day of year 170).

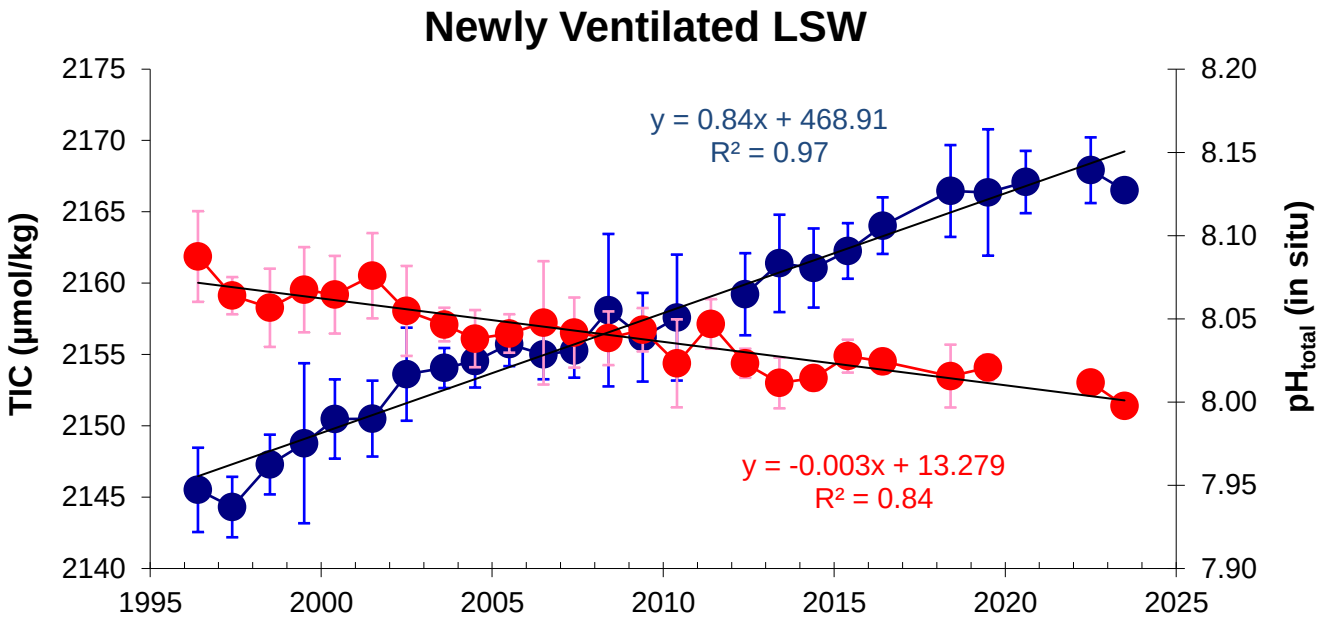

Figure 3. Time series of total inorganic carbon (blue solid circles) and pH (red solid circles) within the Newly-Ventilated Labrador Sea Water defined as 150–500 m in the Central Labrador Sea. Vertical bars indicate one standard deviation and black solid lines correspond to the linear regression of TIC and pH against time in year for stations located in the CLS for the period 1996–2023.

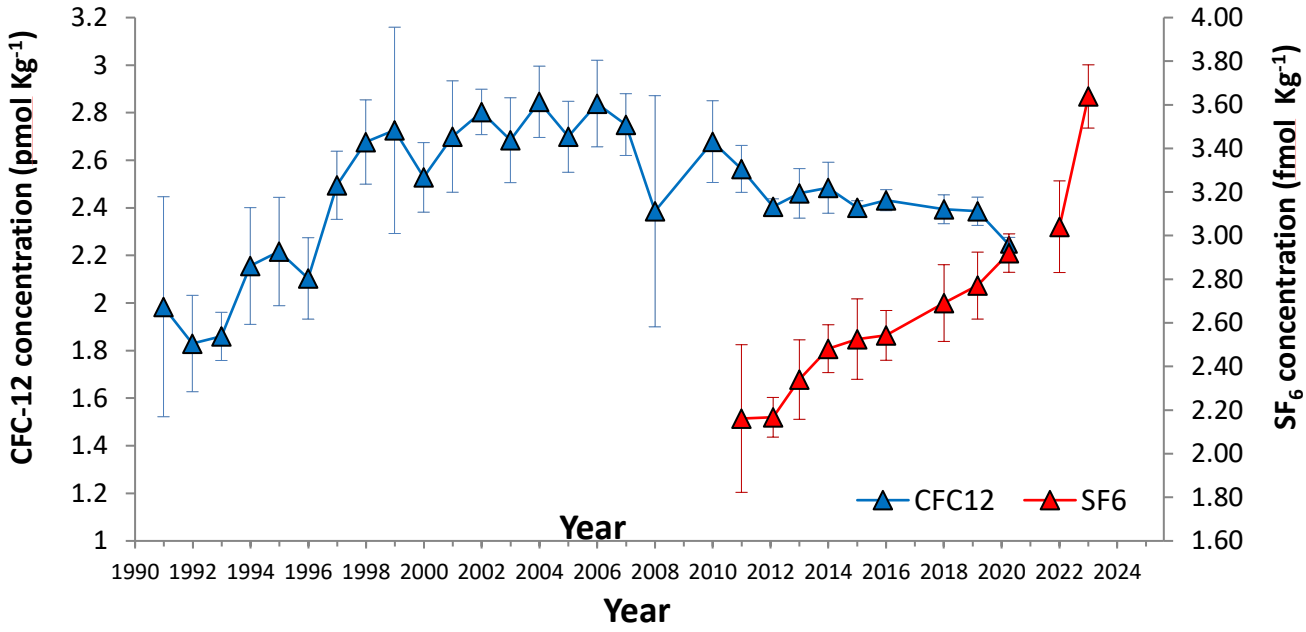

Figure 4. Annual mean concentrations of CFC-12 (blue solid triangles) and SF6 (red solid triangles) in Newly-Ventilated Labrador Sea Water defined as 150–500 m in the Central Labrador Sea from 1991 to 2023. Vertical bars indicate one standard deviation.

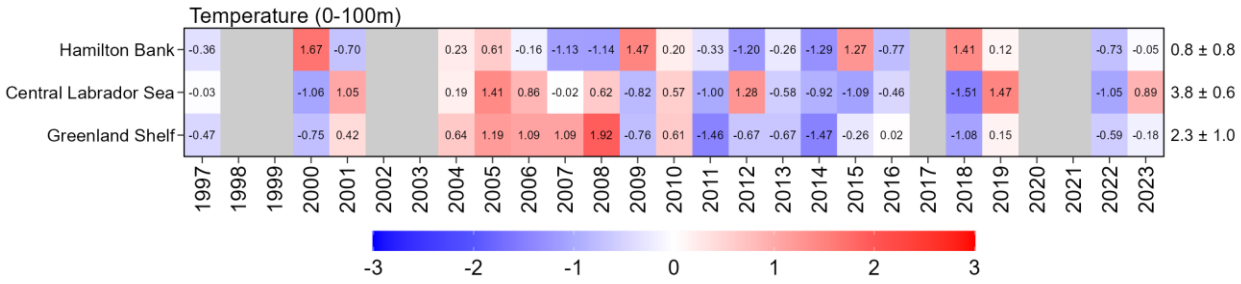

Figure 5. Scorecards for average temperature measured from downcast CTD from surface to 100 m from 1997 to 2023 for the HB, CLS, and GS polygons. Grey boxes indicate no data or late sampling years (not included in the reference period average). Numbers in the scorecards' cells represent the annual standardized anomalies. Numbers on the right side indicate the mean values 1999–2020 (i.e., reference) for a given region as well as the standard deviation (i.e., mean ± standard deviation).

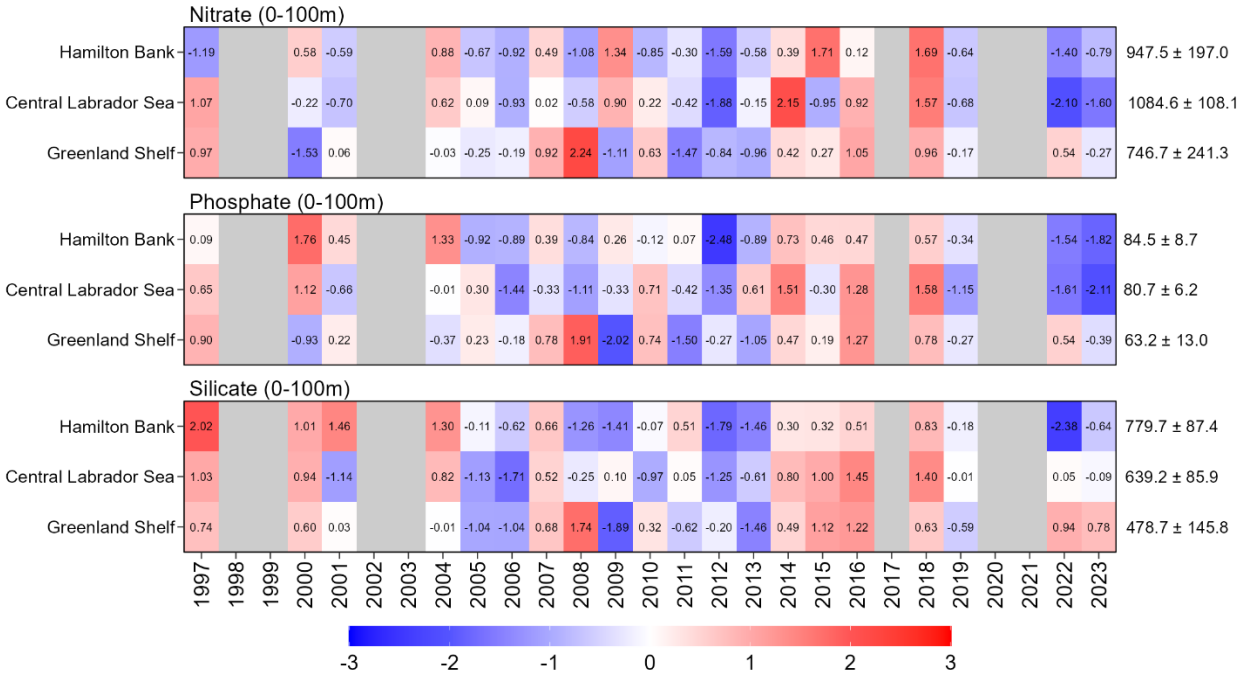

Figure 6. Scorecards for surface nutrients from 1997 to 2023 for the HB, CLS, and GS polygons. Grey boxes indicate no data or late sampling years (not included in the reference period average). Numbers in the scorecards' cells represent the annual standardized anomalies. Numbers on the right side indicate the mean values 1999–2020 (i.e., reference) for a given region as well as the standard deviation (i.e., mean ± standard deviation).

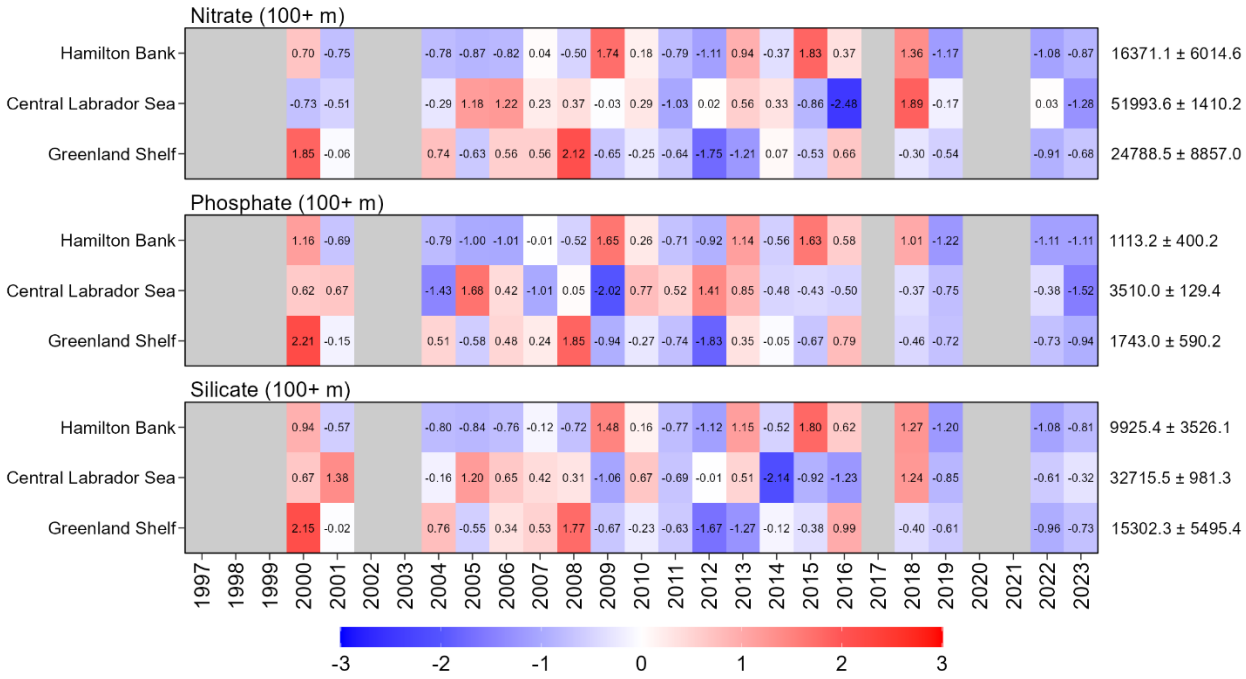

Figure 7. Scorecards for deep nutrients from 1997 to 2023 for the HB, CLS, and GS. Grey boxes indicate no data or late sampling years (not included in the reference period average). Numbers in the scorecards' cells represent the annual standardized anomalies. Numbers on the right side indicate the mean values 1999–2020 (i.e., reference) for a given region as well as the standard deviation (i.e., mean ± standard deviation).

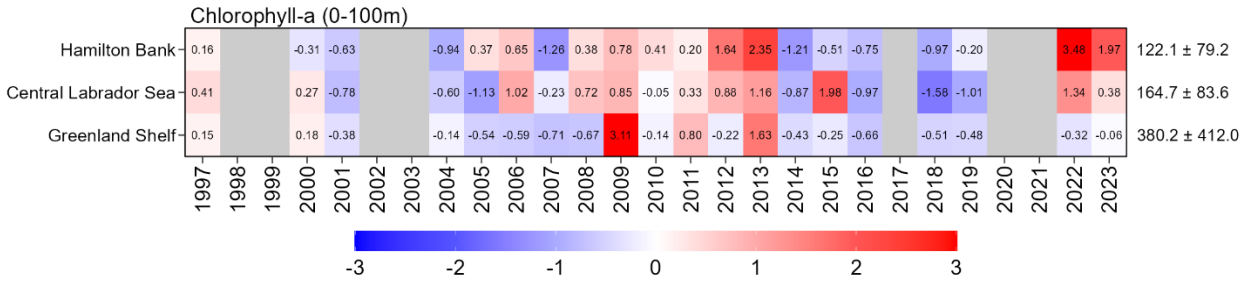

Figure 8. Scorecards from 1997 to 2023 for the HB, CLS, and GS. Grey boxes indicate no data or late sampling years (not included in the reference period average). Numbers within cells represent the annual standardized anomalies. Numbers on the right side indicate the mean values 1999–2020 (i.e., reference) for a given region as well as the standard deviation (i.e., mean ± standard deviation).

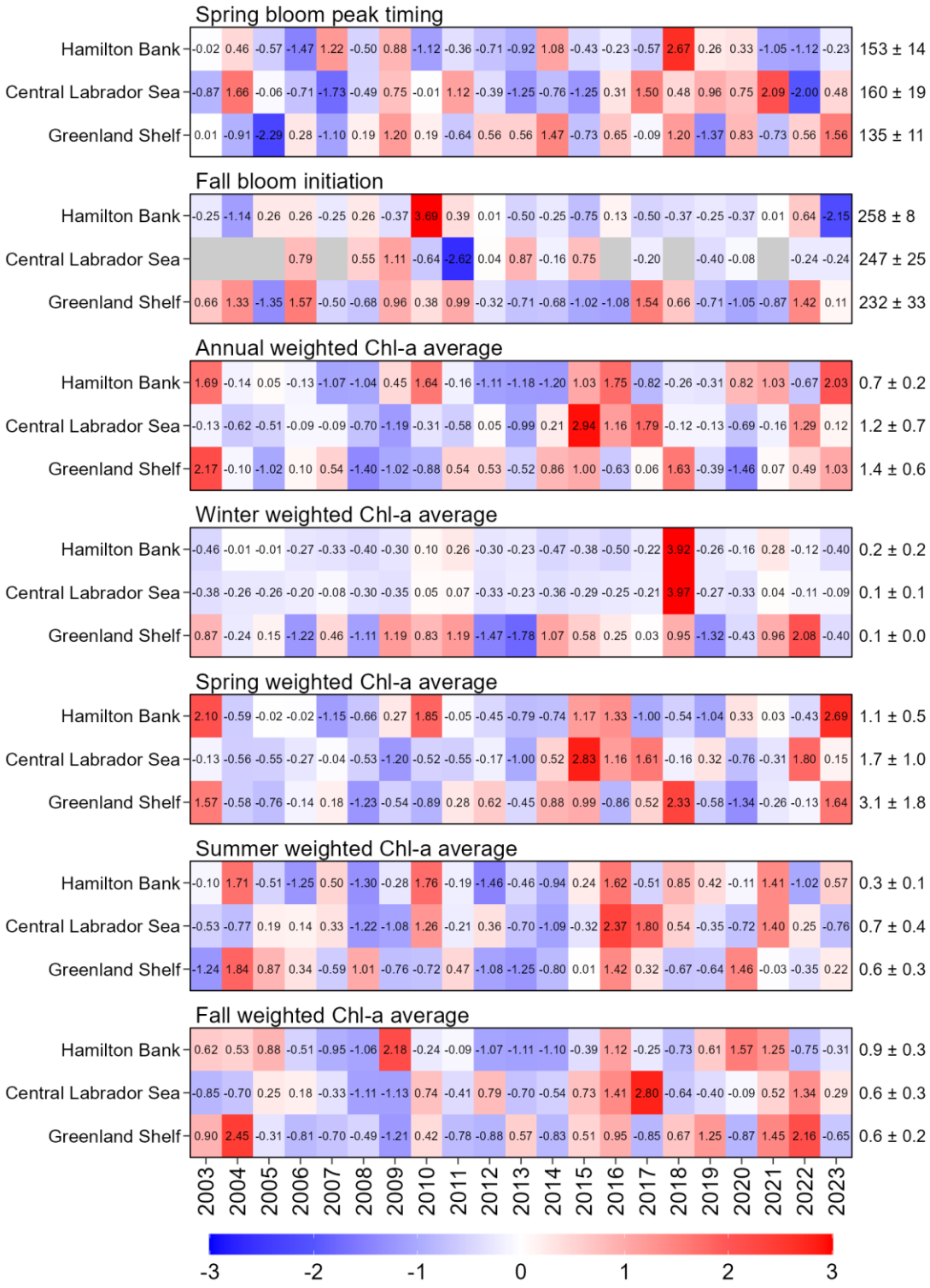

Figure 9. Scorecards for the seasonal chl-a metrics (timing is the day of year, and averages are measured in mg m^{-3}) from 2003 to 2023 for the HB, CLS, and GS polygons. Grey boxes indicate no data. Numbers within cells represent the annual standardized anomalies. Numbers on the right side indicate the mean values 2003–2020 (i.e., reference) for a given region as well as the standard deviation (i.e., mean ± standard deviation).

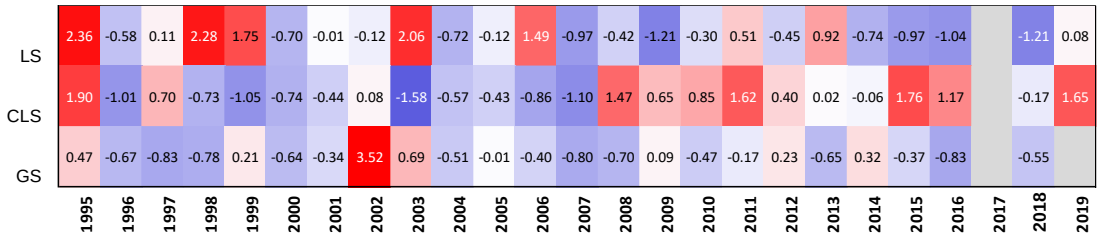

Figure 10. *Calanus finmarchicus*, *C. glacialis*, and *C. hyperboreus* abundances from 1995 to 2019 for the Labrador Shelf (blue), Central Labrador Sea (red), and Greenland Shelf (green). Open circles correspond to years with later-than-normal sampling (i.e., end of June/early July). The dashed lines indicate the average value of the reference period (1999–2010) and vertical bars indicate one standard deviation. The bottom panel shows the same data expressed in normalized anomalies (dimensionless) based on the same reference period. Grey boxes indicate no data. Numbers within cells represent the annual standardized anomalies. Numbers on the right side indicate the mean values 1999–2010 (i.e., reference) for a given region as well as the standard deviation (i.e., mean ± standard deviation).

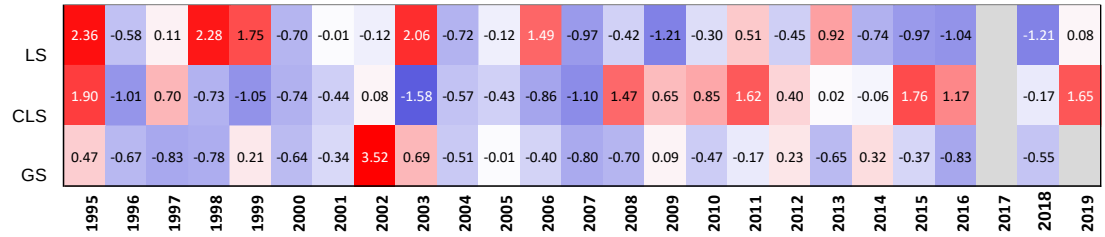

Figure 11. *Pseudocalanus* spp. and *Oithona* spp. anomalies of abundances from 1995 to 2019 for the Labrador Shelf (blue), Central Labrador Sea (red) and Greenland Shelf (green). Open circles correspond to years with later-than-normal sampling (i.e., end of June/early July). The dashed lines indicate the average value of the reference period (1999–2010) and vertical bars indicate one standard deviation. The bottom panel shows the same data expressed in normalized anomalies (dimensionless) based on the same reference period. Grey boxes indicate no data. Numbers on the right side indicate the mean values 1999–2010 (i.e., reference) for a given region as well as the standard deviation (i.e., mean ± standard deviation).

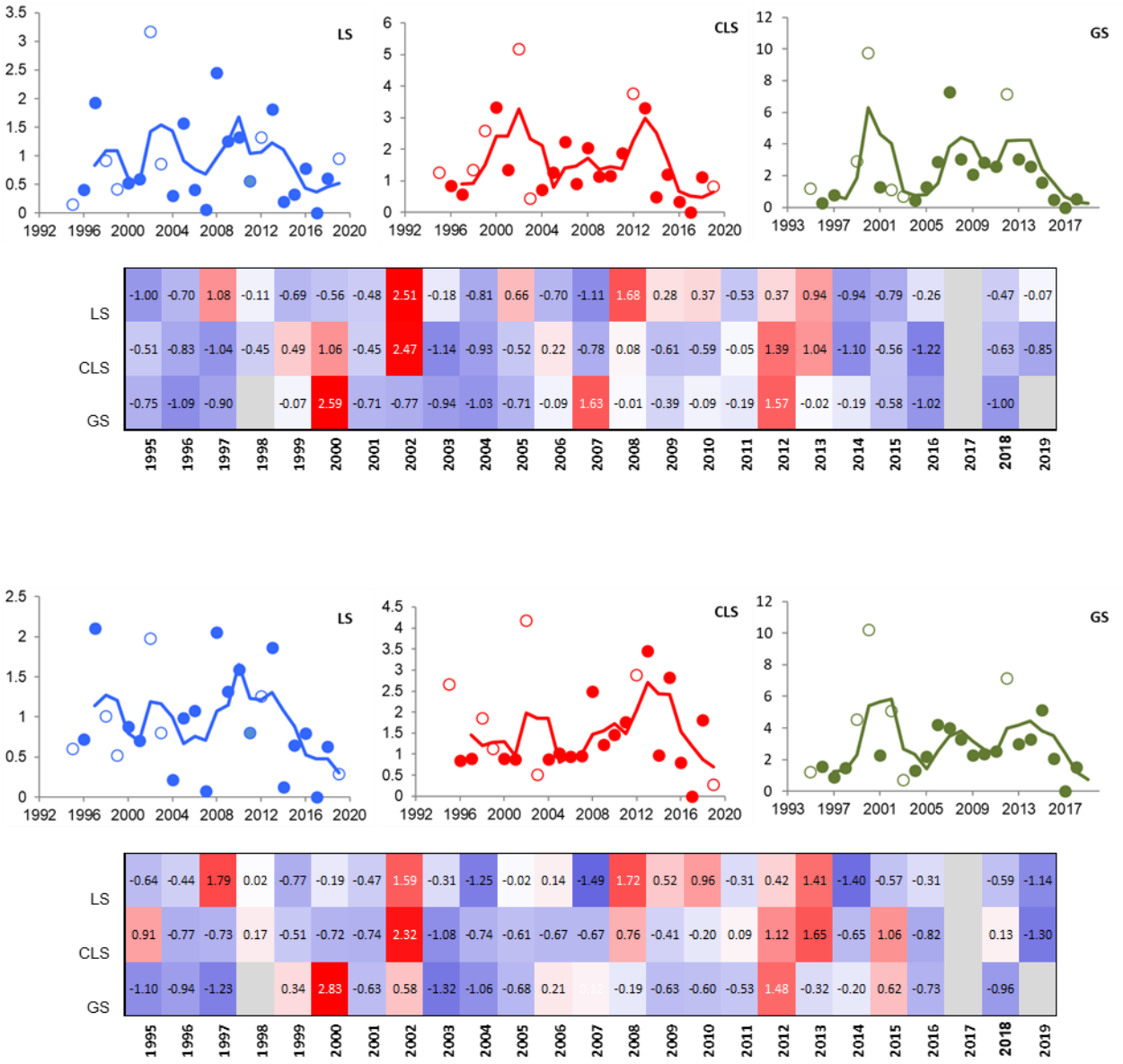

Figure 12. *Euphausiid* and *Hyperiid* (Amphipode) anomalies of abundances from 1995 to 2018 for the Labrador Shelf (blue), Central Labrador Sea (red), and Greenland Shelf (green). Open circles correspond to years with later-than-normal sampling (i.e., end of June/early July). The dashed lines indicate the average value of the reference period (1999–2010) and vertical bars indicate one standard deviation. The bottom panel shows the same data expressed in normalized anomalies (dimensionless) based on the same reference period. Grey boxes indicate no data. Numbers on the right side indicate the mean values 1999–2010 (i.e., reference) for a given region as well as the standard deviation (i.e., mean ± standard deviation).

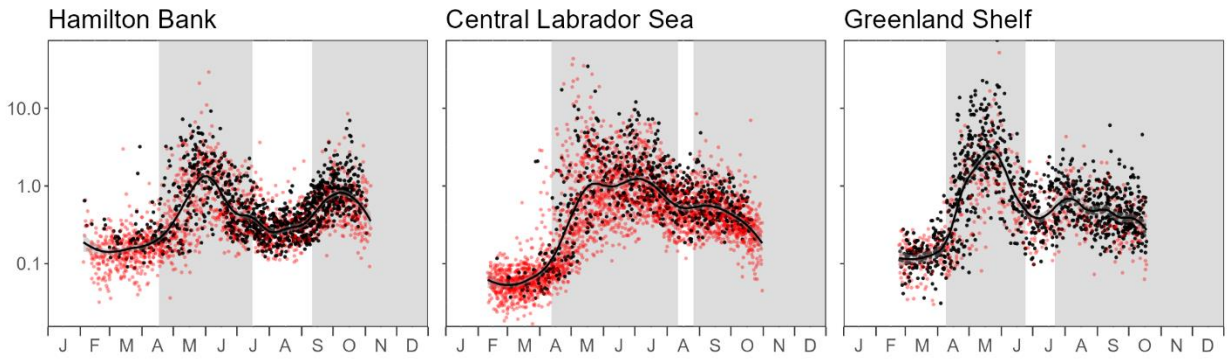

Figure 13. Time series of daily average concentrations within each Labrador Sea polygon over the climatological period (2003-2020). Grey shaded areas indicate the spring and fall bloom periods. White areas indicate the winter and summer periods. Red circles correspond to daily data coverage of less than 20% of a polygon. Days of the year marking the transition from winter to spring, spring to summer, and summer to fall are 107, 197, and 254 (Hamilton Bank), 102, 223, and 238 (Central Labrador Sea), and 99, 175, and 203 (Greenland Shelf).